Integrated Sensing and Communications for Reconfigurable Intelligent Surface-aided Cell-Free Networks

Shanza Shakoor, *Student Member, IEEE,* Quang Nhat Le, *Member, IEEE,* Een-Kee Hong, *Senior Member, IEEE,* Berk Canberk, *Senior Member, IEEE*, and Trung Q. Duong, *Fellow, IEEE*

***Abstract*—This work explores a cell-free integrated sensing and communication (CF-ISAC) framework in which distributed access points work together to support communication users (UEs) with assistance from multiple reconfigurable intelligent surfaces (RISs) while simultaneously performing target sensing. An effective strategy is introduced for the joint optimization of communication parameters, sensing beamforming designs, and reflecting coefficients, with the goal of enhancing the minimum signal-to-interference-plus-noise ratio (SINR) among all UEs. To address the complexity of this non-convex optimization problem, a robust alternating optimization method is designed. The numerical results confirm that the proposed approach significantly boosts the minimum SINR in CF-ISAC systems, demonstrating the advantages of utilizing RISs.**

***Index Terms*—Integrated sensing and communication (ISAC), joint optimization, reconfigurable intelligent surface (RIS).**

I. Introduction

As the demand for faster, more efficient wireless networks grows, the integration of advanced technologies becomes crucial. With the emergence of sixth-generation (6G), wireless systems are expected to deliver significantly higher efficiency and performance, addressing the increasing need for faster data transfer and lower latency [1], [2]. One promising development in this domain is the integrated sensing and communication (ISAC) paradigm, which enables simultaneous communication and environmental sensing.

A major breakthrough in wireless communications is the advent of reconfigurable intelligent surface (RIS) technology, integrated with ISAC, marks a significant milestone in wireless communications by enabling dynamic control of the radio environment, improving signal quality, mitigating interference, and enhancing spectrum efficiency in challenging propagation environments [3]. Several studies have examined the capability of RIS to enhance the efficiency and effectiveness of wireless networks. For example, the authors in [4] demonstrated how RIS beamforming improves the signal-to-interference-plus-noise ratio (SINR) and expands sensing range. Similarly, the work in [5] focused on jointly optimizing RIS beamforming and access point (AP) precoding, aiming to achieve the highest possible minimum beampattern gain in the targeted sensing directions.

Alongside RIS, the concept of cell-free (CF) networks has gained significant attention as an innovative architecture for future wireless systems, where multiple distributed APs provide seamless coverage across large areas, eliminating traditional cell boundaries [6]. This ensures seamless coverage and high data rates, particularly at the edges of the network, where conventional cellular systems struggle [7]. Integrating RIS into CF networks further enhances their performance by dynamically shaping the wireless propagation environment. Through the integration of RIS, the system can achieve improved signal quality, interference mitigation, and better spectral efficiency [8], [9]. The combined system leverages spatial diversity and cooperative transmission, enabling more reliable and efficient communication. Furthermore, the inherent adaptability of RIS in such networks allows for precise control of beamforming and interference patterns, ensuring enhanced network performance, even in dense or challenging environments [10], [11].

Recent studies have explored various optimization techniques to enhance the performance of these advanced technologies. For instance, the authors in [12] investigated a scenario with multiple transmitting APs and a single sensing AP, aiming to optimize the sensing signal-to-noise ratio (SNR) while ensuring that the communication SINR satisfied. Furthermore, the authors in [13] explored the scalability of these systems by considering configurations with multiple transmitting and receiving APs. Moreover, the authors in [14] examined a scenario involving multiple targets.

Despite these advancements, the integration of RIS, ISAC, and CF systems for joint resource optimization remains an underexplored area. RIS and ISAC can considerably improve cell-free networks by enhancing signal coverage, energy efficiency, and interference management through intelligent signal reflection and environmental sensing. Together, they enable more efficient resource allocation, precise user localization, and better overall network performance, reducing the need for extensive infrastructure. However, the challenges associated with combining these technologies, especially in terms of joint communication and sensing beamforming, have yet to be comprehensively addressed. In this paper, we present

S. Shakoor and Q. N. Le are with Memorial University, Canada (e-mail: {sshakoor, qnle}@mun.ca). E.-K. Hong is with Kyung Hee University, South Korea (e-mail: ekhong@khu.ac.kr). B. Canberk is with Edinburgh Napier University, UK (e-mail: b.canberk@napier.ac.uk). T. Q. Duong is with Memorial University, Canada, and with Queen's University Belfast, UK, and also with Kyung Hee University, South Korea (e-mail: tduong@mun.ca). Corresponding authors are Trung Q. Duong and Een-Kee Hong.

The work of T. Q. Duong was supported in part by the Canada Excellence Research Chair (CERC) Program CERC-2022-00109. The work of B. Canberk is supported by The Scientific and Technological Research Council of Turkey (TUBITAK) Frontier RD Laboratories Support Program for BTS Advanced AI Hub: BTS Autonomous Networks and Data Innovation Lab Project 5239903.

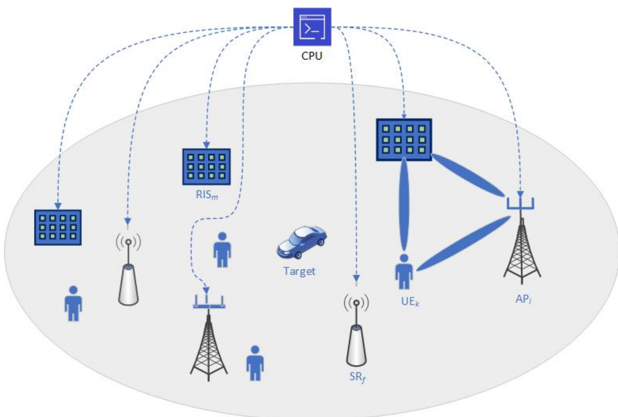

Fig. 1: RIS-aided CF-ISAC system model.

an approach for efficiently optimizing communication and sensing beamforming, along with RIS's reflecting coefficients, to max-min SINR of all communication users (UEs) while meeting sensing SINR requirements. To address this non-convex problem, we employ an alternating optimization (AO) algorithm, which significantly enhances the performance of the integrated system.

A. Notations

We denote vectors using bold lowercase letters and matrices with bold uppercase letters. $\mathbb{C}^{N\times 1}$ signifies the space of $N\times 1$ complex-valued vectors, and $\mathbb{C}^{E\times N}$ denotes the set of $E\times N$ complex-valued matrices. $\mathbf{W}^H$ and $\text{Tr}(\mathbf{W})$ represent the Hermitian transpose and trace of the matrix $\mathbf{W}$, respectively. $\mathbf{W}\succeq 0$ represents that $\mathbf{W}$ is a positive semidefinite matrix. The notation $\texttt{diag}(\psi)$ refers to a diagonal matrix whose diagonal entries correspond to the elements of the vector ψ. The symbols $\|\cdot\|$ and $|\cdot|$ denote the Euclidean norm of a vector and the magnitude of a complex number, respectively. Additionally, $\Re\{\cdot\}$ extracts the real part of a given expression. $\mathbf{I}_M$ represents the $M\times M$ identity matrix.

II. System Model

As illustrated in Fig. 1, the study examines a RIS-assisted CF network, composed of multiple components, including $\mathcal{L}=1,2,\ldots,L$ APs, $\mathcal{M}=1,2,\ldots,M$ RISs, $\mathcal{K}=1,2,\ldots,K$ UEs, $\mathcal{F}=1,2,\ldots,F$ sensing receivers (SRs), along with a single sensing target. Each AP, UE, and SR are possessing with N, single, and D antennas, respectively. Furthermore, each RIS consists of E passive reflecting elements, denoted as $\mathcal{E}\triangleq\{1,2,\cdots,E\}$. A central processing unit (CPU) is employed to oversee control and coordination tasks within the network. All APs and SRs are connected to the CPU through wired backhaul links. Additionally, the management of all RISs is handled either by the CPU or directly by the APs, utilizing either wired or wireless connections to facilitate flexible and efficient control.

A. Transmission Model

The complex baseband signal $\boldsymbol{x}_l\in\mathbb{C}^{N\times 1}$ transmitted by AP$_l$ is defined as

$$\boldsymbol{x}_l=\boldsymbol{w}_{l,0}x_0+\sum_{k\in\mathcal{K}}\boldsymbol{w}_{l,k}x_k, \tag{1}$$

where $x_0\sim\mathcal{CN}(0,1)$ and $x_k\sim\mathcal{CN}(0,1)$ denote the sensing stream and the k-th UE's transmitted symbol, respectively. Here, $\boldsymbol{w}_{l,0}\in\mathbb{C}^{N\times 1}$ and $\boldsymbol{w}_{l,k}\in\mathbb{C}^{N\times 1}$ represent the beamforming vectors for the sensing stream and the k-th UE, respectively.

B. Channel Model

The communication channel from each AP to each UE is characterized by two distinct components, facilitated by M RISs: a direct AP-UE link and M AP-RIS-UE reflected links. Each AP-RIS-UE link is further divided into an AP-RIS link and a RIS-UE link. The equivalent channel $\hat{\mathbf{h}}_{l,k}^H\in\mathbb{C}^{1\times N}$ from the AP$_l$ to the k-th UE, $k\in\mathcal{K}$, can be written as

$$\hat{\mathbf{h}}_{l,k}^H(\boldsymbol{\psi})=\mathbf{h}_{l,k}^H+\sum_{m\in\mathcal{M}}\boldsymbol{\psi}_m^T\texttt{diag}\left(\mathbf{g}_{m,k}^H\right)\mathbf{H}_{l,m}, \tag{2}$$

where the channels from AP$_l$ to the k-th UE, AP$_l$ to RIS$_m$, and RIS$_m$ to the k-th UE are represented by $\mathbf{h}_{l,k}^H\in\mathbb{C}^{1\times N}$, $\mathbf{H}_{l,m}\in\mathbb{C}^{E\times N}$, and $\mathbf{g}_{m,k}^H\in\mathbb{C}^{1\times E}$, respectively. Furthermore, the phase shift matrix for RIS$_m$ $\mathbf{\Phi}_m\in\mathbb{C}^{E\times E}$ is denoted as [15]

$$\mathbf{\Phi}_m\triangleq\texttt{diag}\left(e^{j\theta_{m,1}},e^{j\theta_{m,2}},\ldots,e^{j\theta_{m,E}}\right), \tag{3}$$

where the phase shift of the e-th reflecting element of RIS$_m$ is $\theta_{m,e}\in[0,2\pi)$. The phase shift matrix $\mathbf{\Phi}_m$ can be rewritten as $\mathbf{\Phi}_m=\texttt{diag}\left(\psi_{m,1},\psi_{m,2},\ldots,\psi_{m,E}\right)$, with $|\psi_{m,e}|=1$, $\forall m\in\mathcal{M}$, $\forall e\in\mathcal{E}$. Defining $\boldsymbol{\psi}_m=\left[\psi_{m,1},\psi_{m,2},\ldots,\psi_{m,E}\right]^T$.

C. Signal Processing at the Receivers

The signal y_k received at the k-th UE, $k\in\mathcal{K}$, which can be formulated as

$$y_k=\sum_{l\in\mathcal{L}}\hat{\mathbf{h}}_{l,k}^H\boldsymbol{x}_l+\epsilon_k, \tag{4}$$

where additive white Gaussian noise (AWGN) at the k-th UE is characterized by $\epsilon_k\sim\mathcal{CN}(0,\sigma^2)$. According to (4), the received SINR of the k-th UE can be written as

$$\gamma_k(\boldsymbol{w},\boldsymbol{\psi})=\frac{\left|\hat{\mathbf{h}}_k^H(\boldsymbol{\psi})\boldsymbol{w}_k\right|^2}{\left|\hat{\mathbf{h}}_k^H(\boldsymbol{\psi})\boldsymbol{w}_0\right|^2+\sum\limits_{j\in\mathcal{K}\backslash k}\left|\hat{\mathbf{h}}_k^H(\boldsymbol{\psi})\boldsymbol{w}_j\right|^2+\sigma^2}, \tag{5}$$

where $\boldsymbol{w}\triangleq\{\boldsymbol{w}_{l,0},\boldsymbol{w}_{l,k}\}_{l\in\mathcal{L},k\in\mathcal{K}}$, $\boldsymbol{\psi}\triangleq\{\psi_{m,e}\}_{m\in\mathcal{M},e\in\mathcal{E}}$, $\hat{\mathbf{h}}_k=\left[\hat{\mathbf{h}}_{1,k}^H,\hat{\mathbf{h}}_{2,k}^H,\ldots,\hat{\mathbf{h}}_{L,k}^H\right]^H$, $\boldsymbol{w}_0=\left[\boldsymbol{w}_{1,0}^H,\boldsymbol{w}_{2,0}^H,\ldots,\boldsymbol{w}_{L,0}^H\right]^H$, and $\boldsymbol{w}_k=\left[\boldsymbol{w}_{1,k}^H,\boldsymbol{w}_{2,k}^H,\ldots,\boldsymbol{w}_{L,k}^H\right]^H$. $\gamma_k(\boldsymbol{w},\boldsymbol{\psi})$ denotes the SINR for the k-th UE.

D. Multi-static Sensing

We consider multi-static sensing, in which the CPU collects and processes signals received from all F SRs for target detection [16]. The signal received by the f-th SR is given by

$$\boldsymbol{y}_f=\sum_{l\in\mathcal{L}}\kappa_{f,l}\sqrt{\alpha_{f,l}}\boldsymbol{b}(\varphi_f)\boldsymbol{b}^H(\varphi_l)\boldsymbol{x}_l+\boldsymbol{\epsilon}_f, \tag{6}$$

where $\kappa_{f,l} \sim \mathcal{CN}(0, \sigma_{f,l}^2)$ denotes the radar cross section (RCS) of the target from AP_l to f-th SR, $\alpha_{f,l} = \frac{\lambda_c^2}{(4\pi)^3 d_{f,s}^2 d_{l,s}^2}$ means the channel gain from the AP_l to the sensing target at the distance $d_{l,s}$ and from the target to the f-th SR at the distance $d_{f,s}$, λ_c is the carrier wavelength, $\boldsymbol{b}(\varphi)$ denotes the array response vector such that φ_l/φ_f is the angle of departure/arrival from the target location to the AP_l/f-th SR, and $\boldsymbol{\epsilon}_f \sim \mathcal{CN}(\mathbf{0}, \sigma^2 \mathrm{I}_D) \in \mathbb{C}^{D\times 1}$ is the receiver noise at the f-th SR. By jointly processing the received signal from all SRs, the joint sensing SNR can be derived as

$$\gamma_s(\boldsymbol{w}) = \frac{\sum\limits_{f\in\mathcal{F}}\sum\limits_{l\in\mathcal{L}} \sigma_{f,l}^2 \alpha_{f,l} ||\boldsymbol{b}^H(\varphi_l)\boldsymbol{W}_l||^2}{F\sigma^2}, \tag{7}$$

where $\boldsymbol{W}_l = \left[\boldsymbol{w}_{l,0}, \boldsymbol{w}_{l,1}, \ldots, \boldsymbol{w}_{l,K}\right] \in \mathbb{C}^{N\times(K+1)}$ concatenates the beamforming vectors of all UEs and the sensing target.

E. Problem Formulation

The objective is to maximize the minimum SINR γ_k across all UEs through the joint optimization of variables $(\boldsymbol{w}, \boldsymbol{\psi})$. The optimization problem is defined as follows:

$$\max_{\boldsymbol{w},\boldsymbol{\psi}} \quad \min_{k\in\mathcal{K}} \gamma_k(\boldsymbol{w}, \boldsymbol{\psi}) \tag{8a}$$

$$\text{s.t.} \quad ||\boldsymbol{w}_{l,0}||^2 + \sum_{k\in\mathcal{K}} ||\boldsymbol{w}_{l,k}||^2 \le P_l^{\max}, \forall l \in \mathcal{L}, \tag{8b}$$

$$\gamma_k(\boldsymbol{w}, \boldsymbol{\psi}) \ge \gamma_k^{\min}, \forall k \in \mathcal{K}, \tag{8c}$$

$$\gamma_s(\boldsymbol{w}) \ge \gamma_s^{\min}, \tag{8d}$$

$$|\psi_{m,e}| = 1, \forall m \in \mathcal{M}, \forall e \in \mathcal{E}. \tag{8e}$$

where $\gamma_k^{\min}$ and $\gamma_s^{\min}$ are the minimum SINR threshold for k-th UE and sensing target, respectively, and $P_l^{\max}$ is the transmit power limit for the AP_l. The non-concave objective function (8a), the non-convex constraints (8c) and (8d), the unit-modulus constraints (8e), and the mutually connected variables $\boldsymbol{w}$ and $\boldsymbol{\psi}$ let problem (8) become a highly challenging non-convex problem, which is difficult to address.

III. Proposed Solution

In each iteration, let $(\boldsymbol{\psi}^{(\eta)}, \boldsymbol{w}^{(\eta)})$ denote the feasible solution for problem (8) obtained from the $(\eta-1)$-th round. We propose an efficient alternating optimization algorithm to address (8): at iteration $\eta+1$, the algorithm first optimizes $\boldsymbol{w}$ by solving (8) with $\boldsymbol{\psi}^{(\eta)}$ fixed to obtain $\boldsymbol{w}^{(\eta+1)}$, and then optimizes $\boldsymbol{\psi}$ by solving (8) with $\boldsymbol{w}^{(\eta+1)}$ fixed to obtain $\boldsymbol{\psi}^{(\eta+1)}$.

A. Beamforming Optimization

At the iteration $\eta+1$, problem (8) with the given $\boldsymbol{\psi}^{(\eta)}$ can be defined as

$$\max_{\boldsymbol{w},\tau} \quad \tau \tag{9a}$$

$$\text{s.t.} \quad \gamma_k(\boldsymbol{w}, \boldsymbol{\psi}^{(\eta)}) \ge \tau, \forall k \in \mathcal{K}, \tag{9b}$$

$$||\boldsymbol{w}_{l,0}||^2 + \sum_{k\in\mathcal{K}} ||\boldsymbol{w}_{l,k}||^2 \le P_l^{\max}, \forall l \in \mathcal{L}, \tag{9c}$$

$$\tau \ge \gamma_k^{\min}, \forall k \in \mathcal{K}, \tag{9d}$$

$$\gamma_s(\boldsymbol{w}) \ge \gamma_s^{\min}, \tag{9e}$$

where τ is a slack variable. The constraints (9b) and (9e) are non-convex. To tackle the non-convexity of (9b), we transform it into a convex counterpart by leveraging an auxiliary variable $\boldsymbol{\aleph} \triangleq \{\aleph_k\}_{\forall k}$ as

$$\tau\aleph_k \le \mathrm{Tr}\big(\mathbf{h}_k^H(\boldsymbol{\psi}^{(\eta)})\mathbf{w}_k\mathbf{w}_k^H\mathbf{h}_k(\boldsymbol{\psi}^{(\eta)})\big), \tag{10a}$$

$$\aleph_k \ge \left|\hat{\mathbf{h}}_k^H(\boldsymbol{\psi}^{(\eta)})\boldsymbol{w}_0\right|^2 + \sum_{j\in\mathcal{K}\backslash k} \left|\hat{\mathbf{h}}_k^H(\boldsymbol{\psi}^{(\eta)})\boldsymbol{w}_j\right|^2 + \sigma^2. \tag{10b}$$

The upper bound of $\tau\aleph_k$ can be expressed as

$$\tau\aleph_k \le \frac{\tau^{(\eta)}}{2\aleph_k^{(\eta)}}\aleph_k^2 + \frac{\aleph_k^{(\eta)}}{2\tau^{(\eta)}}\tau^2, \forall k \in \mathcal{K}, \tag{11}$$

where $\tau^{(\eta)}$ and $\aleph_k^{(\eta)}$, $\forall k \in \mathcal{K}$, are the obtained values at the η-th iteration. Hence, (10a) can be convexified as

$$\frac{\tau^{(\eta)}}{2\aleph_k^{(\eta)}}\aleph_k^2 + \frac{\aleph_k^{(\eta)}}{2\tau^{(\eta)}}\tau^2 \le \mathrm{Tr}\big(\mathbf{h}_k^H(\boldsymbol{\psi}^{(\eta)})\mathbf{w}_k\mathbf{w}_k^H\mathbf{h}_k(\boldsymbol{\psi}^{(\eta)})\big), \forall k \in \mathcal{K}. \tag{12}$$

To deal with the non-convex constraint (9e), the following inequality $||\boldsymbol{p}||^2 \ge 2\Re\{(\boldsymbol{p}^{(\eta)})^H\boldsymbol{p}\} - ||\boldsymbol{p}^{(\eta)}||^2$ is used to convexify the numerator term of $\gamma_s(\boldsymbol{w})$. Thus, $\gamma_s(\boldsymbol{w})$ can be rewritten as (13) at the beginning of the next page, such that

$$\gamma_s^{(\eta)}(\boldsymbol{w}) \ge \gamma_s^{\min}. \tag{14}$$

Finally, the convex approximation of problem (9) at iteration $\eta+1$ is formulated as

$$\max_{\boldsymbol{w},\tau,\boldsymbol{\aleph}} \quad \tau \tag{15a}$$

$$\text{s.t.} \quad (9c), (9d), (12), (14). \tag{15b}$$

B. Phase Shift Optimization

At the iteration $\eta+1$, for given $\boldsymbol{w}^{(\eta+1)}$, problem (8) can be expressed as

$$\max_{\boldsymbol{\psi},\upsilon} \quad \upsilon \tag{16a}$$

$$\text{s.t.} \quad \gamma_k(\boldsymbol{w}^{(\eta+1)}, \boldsymbol{\psi}) \ge \upsilon, \forall k \in \mathcal{K}, \tag{16b}$$

$$\upsilon \ge \gamma_k^{\min}, \forall k \in \mathcal{K}, \tag{16c}$$

$$|\psi_{m,e}| \le 1, \forall m \in \mathcal{M}, \forall e \in \mathcal{E}, \tag{16d}$$

where υ is a slack variable. The non-convex fractional constraint (16b) presents significant challenges in solving problem (16). To address this, we utilize Dinkelbach's transformation, which reformulates the constraint into a more manageable polynomial form [17]. This approach allows efficient handling of the original fractional constraint. Specifically, the transformation converts the fractional constraint (16b) into an equivalent but more analytically favorable polynomial expression, simplifying the optimization process, which is expressed as

$$\left|\mathbf{h}_k^H(\boldsymbol{\psi})\mathbf{w}_k^{(\eta+1)}\right|^2 - \zeta_k\left(\left|\mathbf{h}_k^H(\boldsymbol{\psi})\mathbf{w}_0^{(\eta+1)}\right|^2 + \sum_{j\in\mathcal{K}\backslash\{k\}} \left|\mathbf{h}_k^H(\boldsymbol{\psi})\mathbf{w}_j^{(\eta+1)}\right|^2 + \sigma^2\right) \ge \upsilon, \forall k \in \mathcal{K}, \tag{17}$$

$$\gamma_s^{(\eta)}(\boldsymbol{w}) := \frac{\sum\limits_{f\in\mathcal{F}}\sum\limits_{l\in\mathcal{L}} \sigma_{f,l}^2 \alpha_{f,l}\big(2\Re\{(\boldsymbol{W}_l^{(\eta)})^H \boldsymbol{b}(\varphi_l)\boldsymbol{b}^H(\varphi_l)\boldsymbol{W}_l\} - ||\boldsymbol{b}^H(\varphi_l)\boldsymbol{W}_l^{(\eta)}||^2\big)}{F\sigma^2}, \tag{13}$$

where ζ_k, $\forall k \in \mathcal{K}$, is the auxiliary variable, whose optimal values can be determined as follows:

$$\zeta_k = \frac{\left|\hat{\mathbf{h}}_k^H(\boldsymbol{\psi})\boldsymbol{w}_k^{(\eta+1)}\right|^2}{\left|\hat{\mathbf{h}}_k^H(\boldsymbol{\psi})\boldsymbol{w}_0^{(\eta+1)}\right|^2 + \sum\limits_{j\in\mathcal{K}\backslash k}\left|\hat{\mathbf{h}}_k^H(\boldsymbol{\psi})\boldsymbol{w}_j^{(\eta+1)}\right|^2 + \sigma^2}, \forall k \in \mathcal{K}. \tag{18}$$

Next, for brevity, we define $\mathbf{p}_{k,j} = \mathrm{diag}(\mathbf{g}_k^H)\mathbf{H}\mathbf{w}_j^{(\eta+1)}$, $\mathbf{q}_{k,j} = \mathbf{h}_k^H\mathbf{w}_j^{(\eta+1)}$, and $\bar{\mathcal{K}} = \mathcal{K} \cup \{0\}$, where $\mathbf{h}_k = \left[\mathbf{h}_{1,k}^H, \mathbf{h}_{2,k}^H, \ldots, \mathbf{h}_{L,k}^H\right]^H$, $\boldsymbol{\psi} = \left[\boldsymbol{\psi}_1^T, \boldsymbol{\psi}_2^T, \ldots, \boldsymbol{\psi}_M^T\right]^T$, $\mathbf{g}_k = \left[\mathbf{g}_{1,k}^H, \mathbf{g}_{2,k}^H, \ldots, \mathbf{g}_{M,k}^H\right]^H$, $\mathbf{H}_l = \left[\mathbf{H}_{l,1}^H, \mathbf{H}_{l,2}^H, \ldots, \mathbf{H}_{l,M}^H\right]^H$, and $\mathbf{H} = [\mathbf{H}_1, \mathbf{H}_2, \ldots, \mathbf{H}_L]$. The constraint in (17) is reformulated as

$$\begin{aligned}\left|\boldsymbol{\psi}^T\mathbf{p}_{k,k} + \mathbf{q}_{k,k}\right|^2 - \zeta_k\left(\sum_{j\in\bar{\mathcal{K}}\backslash\{k\}}\left|\boldsymbol{\psi}^T\mathbf{p}_{k,j} + \mathbf{q}_{k,j}\right|^2 + \sigma^2\right)\\ \geq \upsilon, \forall k \in \mathcal{K}.\end{aligned} \tag{19}$$

The quadratic function $\left|\boldsymbol{\psi}^T\mathbf{p}_{k,k} + \mathbf{q}_{k,k}\right|^2$ in (19) remains non-convex with respect to $\boldsymbol{\psi}$. To overcome this challenge, we intend to derive a convex surrogate function that serves as a local lower bound by employing the majorization-minimization (MM) technique. At the iteration $\eta + 1$, the surrogate function for $\left|\boldsymbol{\psi}^T\mathbf{p}_{k,k} + \mathbf{q}_{k,k}\right|^2$ is derived via the first-order Taylor expansion, illustrated as

$$\begin{aligned}&\left|\boldsymbol{\psi}^T\mathbf{p}_{k,k} + \mathbf{q}_{k,k}\right|^2\\ &= \boldsymbol{\psi}^T\mathbf{p}_{k,k}\mathbf{p}_{k,k}^H\boldsymbol{\psi}^\star + 2\Re\left\{\mathbf{q}_{k,k}\mathbf{p}_{k,k}^H\boldsymbol{\psi}^\star\right\} + \left|\mathbf{q}_{k,k}\right|^2 \geq \boldsymbol{\psi}_{\eta+1}^T\mathbf{p}_{k,k}\mathbf{p}_{k,k}^H\\ &\times\boldsymbol{\psi}_{\eta+1}^\star + 2\Re\left\{\boldsymbol{\psi}_{\eta+1}^T\mathbf{p}_{k,k}\mathbf{p}_{k,k}^H(\boldsymbol{\psi}^\star - \boldsymbol{\psi}_{\eta+1}^\star)\right\} + 2\Re\left\{\mathbf{q}_{k,k}^H\mathbf{p}_{k,k}^H\boldsymbol{\psi}^\star\right\}\\ &+ \left|\mathbf{q}_{k,k}\right|^2.\end{aligned} \tag{20}$$

By plugging the result (20) into (19), the constraint (16b) can be reformulated as

$$\begin{aligned}&2\Re\left\{\boldsymbol{\psi}_{\eta+1}^T\mathbf{p}_{k,k}\mathbf{p}_{k,k}^H(\boldsymbol{\psi}^\star - \boldsymbol{\psi}_{\eta+1}^\star)\right\} + 2\Re\left\{\mathbf{q}_{k,k}\mathbf{p}_{k,k}^H\boldsymbol{\psi}^\star\right\}\\ &- \zeta_k\left(\sum_{j\in\bar{\mathcal{K}}\backslash\{k\}}\left|\boldsymbol{\psi}^T\mathbf{p}_{k,k} + \mathbf{q}_{k,k}\right|^2 + \sigma^2\right) + \boldsymbol{\psi}_{\eta+1}^T\mathbf{p}_{k,k}\mathbf{p}_{k,k}^H\boldsymbol{\psi}_{\eta+1}^\star\\ &+ \left|\mathbf{q}_{k,k}\right|^2 \geq \upsilon, \forall k \in \mathcal{K}.\end{aligned} \tag{21}$$

Thus, the convexified form of problem (16) for iteration $\eta+1$ is described as

$$\max_{\boldsymbol{\psi},\upsilon} \quad \upsilon \tag{22a}$$

$$\text{s.t.} \quad (16c), (16d), (21). \tag{22b}$$

The proposed alternating optimization algorithm is summarized in Algorithm 1.

Algorithm 1 Alternating Optimization for Problem (8)

Require: Initialize $\eta := 0$ and compute an initial feasible point $(\boldsymbol{\psi}^{(0)}, \boldsymbol{w}^{(0)})$.
1: **repeat**
2: With $\boldsymbol{\psi}^{(\eta)}$, solve the convex optimization problem (15) to obtain the optimal solution $\boldsymbol{w}^\star$; update $\boldsymbol{w}^{(\eta+1)} := \boldsymbol{w}^\star$.
3: **repeat**
4: With $\boldsymbol{w}^{(\eta+1)}$, solve the convex optimization problem (22) to compute the optimal solution $\boldsymbol{\psi}^\star$; update $\boldsymbol{\psi}^{(\eta+1)} := \boldsymbol{\psi}^\star$.
5: Update $\zeta_k, \forall k \in \mathcal{K}$ by (18).
6: **until** Convergence
7: Increment $\eta := \eta + 1$.
8: **until** Convergence
9: **return** $(\boldsymbol{\psi}^{(\eta)}, \boldsymbol{w}^{(\eta)})$

IV. Simulation Results

This section presents simulation results to illustrate the performance of RIS-aided CF-ISAC systems. We consider $L = 4$ distributed APs, $K = 3$ UEs, $M = 4$ RISs, $F = 4$ SRs, and $T = 1$ sensing target. Both the UEs and the sensing target are equipped with a single antenna. Both AP and SR are equipped with $N = D = 5$ antennas. Each RIS consists of $E = 8$ passive reflecting elements. The transmit power for each AP is limited to $P_l^{\max} = 1$ W, $\sigma^2 = -80$ dBm. The communication and sensing SINR thresholds are set to be $\gamma_k^{\min} = \gamma_s^{\min} = 1$. Within a circular area of 1 km radius, all APs, UEs, RISs, and SRs are uniformly distributed. We evaluate the performance of Algorithm 1 against two baseline schemes: i) a CF network without RISs and ii) a collocated network with RISs. In the collocated network, a single AP is centrally located within the area to serve all UEs. The AP is equipped with LN antennas and has a maximum transmit power of $LP_l^{\max}$.

Fig. 2 presents the minimum SINR convergence trend of Algorithm 1. On average, the algorithm converges to the optimal value within approximately six iterations, with the minimum SINR stabilizing at 7.38 dB and 8.38 dB for $M = 2$ and $M = 4$, respectively, demonstrating the efficiency of the proposed method. As expected, increasing the number of RISs significantly improves the minimum SINR by 13.54%, thus confirming the advantage of RIS integration in CF-ISAC systems.

Fig. 3 depicts the relationship between the minimum SINR and the number of elements in the RIS. Clearly, the minimum SINR improves significantly with the increase in RIS's elements across CF with RIS and collocated with RIS cases, due to the greater degree of freedom and diversity gain offered by the additional elements in shaping the wireless environment. Moreover, the minimum SINR of the CF-ISAC system with

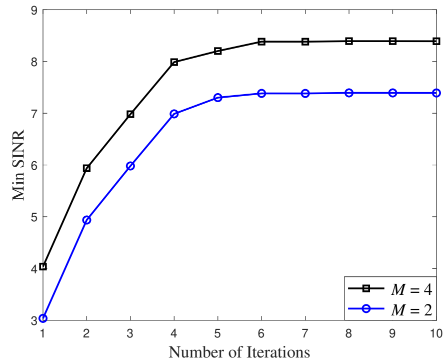

Fig. 2: Convergence behavior of Algorithm 1.

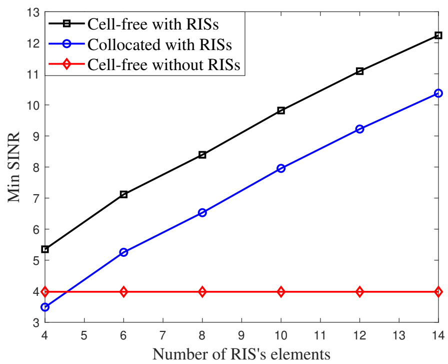

Fig. 3: The effect of number of RIS's elements on the minimum SINR of UEs.

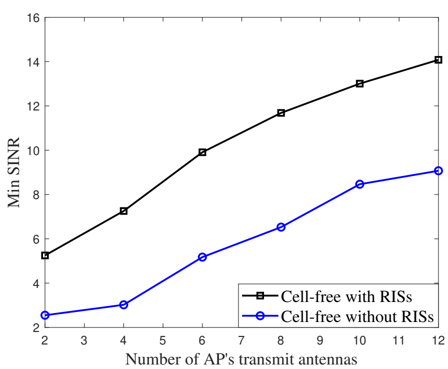

Fig. 4: The impact of number of AP's transmit antennas on the minimum SINR of UEs.

RISs is notably superior to that of the collocated network with RISs, showing an improvement of 28.54% when $E = 8$. This improvement arises because the distributed APs in the CF network position service antennas nearer to the UEs, reducing path losses and offering a greater degree of macro-diversity compared to the collocated network. In addition, the CF-ISAC system with RISs delivers a 110% higher minimum SINR than that of the system without RISs. This highlights the role of RISs in improving the minimum SINR of CF-ISAC system.

Fig. 4 illustrates the effect of the BS's antennas on the minimum SINR. As expected, increasing N results in a higher minimum SINR for both CF-ISAC with RISs and CF-ISAC without RISs schemes. This is because adding more antennas at the APs provides increased spatial diversity and greater beamforming gains. Additionally, the proposed scheme demonstrates a 91% improvement at $N = 6$, considerably outperforms the CF-ISAC without RISs in terms of minimum SINR.

V. Conclusion

This paper has addressed the problem of maximizing the minimum SINR of communication UEs in CF-ISAC networks assisted by multiple RISs. The objective is to simultaneously optimize the transmit beamformers at APs and the reflection coefficients at RISs, ensuring that both communication and sensing SINR constraints are satisfied. This is formulated as a nonconvex optimization problem, which is tackled using an efficient alternating optimization algorithm. Numerical analysis validates the efficiency of the proposed algorithm and underscores the advantages of CF and RIS when contrasted with collocated networks.

References

[1] Q. Xue *et al.*, "A survey of beam management for mmWave and THz communications towards 6G," *IEEE Commun. Surv. Tutor.*, vol. 26, no. 3, pp. 1520–1559, Feb. 2024.

[2] W. Jiang *et al.*, "Terahertz communications and sensing for 6G and beyond: A comprehensive review," *IEEE Commun. Surv. Tutor.*, vol. 26, no. 4, pp. 2326–2381, Apr. 2024.

[3] W. Lyu *et al.*, "CRB minimization for RIS-aided mmWave integrated sensing and communications," *IEEE Internet Things J.*, vol. 11, no. 10, pp. 18 381–18 393, May 2024.

[4] K. Chen-Hu, G. C. Alexandropoulos, and A. García Armada, "Differential data-aided beam training for RIS-empowered multi-antenna communications," *IEEE Access*, vol. 10, pp. 113 200–113 213, Oct. 2022.

[5] R. Liu, M. Li, and A. L. Swindlehurst, "Joint beamforming and reflection design for RIS-assisted ISAC systems," in *Proc. IEEE 30th Eur. Signal Process. Conf.*, Oct. 2022, pp. 997–1001.

[6] E. Shi *et al.*, "RIS-aided cell-free massive MIMO systems for 6G: Fundamentals, system design, and applications," *Proc. IEEE*, vol. 112, no. 4, pp. 331–364, Apr. 2024.

[7] W. Mao *et al.*, "Communication-sensing region for cell-free massive MIMO ISAC systems," *IEEE Trans. Wirel. Commun.*, vol. 23, no. 9, pp. 12 396–12 411, Sep. 2024.

[8] X. Ma *et al.*, "Cooperative beamforming for RIS-aided cell-free massive MIMO networks," *IEEE Trans. Wirel. Commun.*, vol. 22, no. 11, pp. 7243–7258, Nov. 2023.

[9] J. Yao *et al.*, "Robust beamforming design for RIS-aided cell-free systems with CSI uncertainties and capacity-limited backhaul," *IEEE Trans. Commun.*, vol. 71, no. 8, pp. 4636–4649, Aug. 2023.

[10] B. Al-Nahhas, M. Obeed, A. Chaaban, and M. J. Hossain, "RIS-aided cell-free massive MIMO: Performance analysis and competitiveness," in *Proc. IEEE Int. Conf. Commun. Workshops (ICC Workshops)*, June 2021, pp. 1–6.

[11] R. Zhang *et al.*, "Channel training-aided target sensing for terahertz integrated sensing and massive MIMO communications," *IEEE Internet Things J.*, pp. 1–17, Aug. 2024.

[12] U. Demirhan and A. Alkhateeb, "Cell-free ISAC MIMO systems: Joint sensing and communication beamforming," *IEEE Trans. Commun.*, pp. 1–15, Nov. 2024.

[13] S. Buzzi, C. D'Andrea, and S. Liesegang, "Scalability and implementation aspects of cell-free massive MIMO for ISAC," in *2024 19th International Symposium on Wireless Communication Systems (ISWCS)*, Aug. 2024, pp. 1–6.

[14] M. Elfiatoure, M. Mohammadi, H. Q. Ngo, and M. Matthaiou, "Multiple-target detection in cell-free massive MIMO-assisted ISAC," *arXiv preprint arXiv:2404.17263*, pp. 1–13, Apr. 2024.

[15] A. Abdelaziz Salem *et al.*, "Integrated cooperative sensing and communication for RIS-enabled full-duplex cell-free MIMO systems," *IEEE Trans. Commun.*, pp. 1–16, Nov. 2024.

[16] A. A. Nasir, "Joint users' secrecy rate and target's sensing SNR maximization for a secure cell-free ISAC system," *IEEE Commun. Letters*, vol. 28, no. 7, pp. 1549–1553, July 2024.

[17] J. Chu *et al.*, "Joint beamforming and reflection design for secure RIS-ISAC systems," *IEEE Trans. Veh. Tech.*, vol. 73, no. 3, pp. 4471–4475, Mar. 2024.